



# Ruthenium(II)-polypyridyl zirconium(IV) metal-organic frameworks as a new class of sensitized solar cells†

W. A. Maza, A. J. Haring, S. R. Ahrenholtz, C. C. Epley, S. Y. Lin and A. J. Morris\*

A series of Ru(II)L<sub>2</sub>L' (L = 2,2'-bipyridyl, L' = 2,2'-bipyridine-5,5'-dicarboxylic acid), RuDCBPY, -containing zirconium(IV) coordination polymer thin films have been prepared as sensitizing materials for solar cell applications. These metal-organic framework (MOF) sensitized solar cells, MOFSCs, each are shown to generate photocurrent in response to simulated 1 sun illumination. Emission lifetime measurements indicate the excited state quenching of RuDCBPY at the MOF-TiO<sub>2</sub> interface is extremely efficient (>90%), presumably due to electron injection into TiO<sub>2</sub>. A mechanism is proposed in which RuDCBPY-centers photo-excited within the MOF-bulk undergo isotropic energy migration up to 25 nm from the point of origin. This work represents the first example in which a MOFSC is directly compared to the constituent dye adsorbed on TiO<sub>2</sub> (DSC). Importantly, the MOFSCs outperformed their RuDCBPY-TiO<sub>2</sub> DSC counterpart under the conditions used here and, thus, are solidified as promising solar cell platforms.

Received 29th April 2015

Accepted 13th October 2015

DOI: 10.1039/c5sc01565k

[www.rsc.org/chemicalscience](http://www.rsc.org/chemicalscience)

## Introduction

Metal-organic frameworks (MOFs) have shown considerable promise for a number of different applications including gas storage and separation, electro- and photo-catalysis, electrical and optical sensing, as well as photovoltaic applications.<sup>1–10</sup> Incorporation of photoactive ligands into the backbone of the material or by encapsulation within the pores of the material may impart additional reactivity due to the natures of their excited states. Indeed, a number of examples have been reported so far and, more recently, reviewed.<sup>4,11–23</sup>

In particular, MOFs containing photoactive ligands or guest molecules have been designed and characterized as potential materials for photovoltaic applications.<sup>24–32</sup> This includes their use as scaffolds or hosts for commercially available dyes for use as dye-sensitized solar cells (DSCs). The extraordinarily large surface areas afforded by MOFs offer even higher population densities of dye atop TiO<sub>2</sub>, while their spatially rigid and size restrictive pores can minimize deleterious effects due to dye aggregation. These MOF-based cells participating as dye hosts have shown power conversion efficiencies (PCEs,  $\eta$ ) up to ~5%.<sup>29,33</sup> However, the materials explored in these reports are limited by effusion of the dyes from the material bulk.

Commercially available MOFs containing aromatic ligands have been explored for their photovoltaic competence.<sup>29,30,32,34,35</sup>

These include materials comprised of the benzene derivatives terephthalic acid and benzenetricarboxylic acid. Although the short-lived singlet excited states of benzene-type ligands lie well outside the visible region, some evidence suggests very fast (<10 ns) formation of a charge separated state upon UV-excitation.<sup>30</sup> More recently, a 2D coordination polymer thin film photovoltaic device comprised of porphyrinic linkers and Zn(II)-oxo nodes has been prepared by liquid-phase epitaxy.<sup>36</sup> However, these materials demonstrate poor PCEs – typically less than 1%.

The high efficiency of ruthenium(II) polypyridyl dyes in DSCs (PCEs of up to 12%) has instigated incorporation of similar transition metal coordination complexes into MOF sensitized solar cells (MOFSCs) by encapsulation.<sup>37–40</sup> A variety of different MOFs have been modified with ruthenium complexes as either structural supports or *via* encapsulation.<sup>12,13,15,41–47</sup> Lin and co-workers have recently synthesized a water stable zirconium(IV) biphenyldicarboxylic acid metal-organic framework in which ruthenium(II) bis-(2,2'-bipyridine)(2,2'-bipyridine-5,5'-dicarboxylic acid), RuDCBPY, was heterogeneously incorporated into the structural backbone of the framework.<sup>25</sup> At low doping concentrations, it was found that the excited state properties of the RuDCBPY-doped UiO-67 material resembled that of RuDCBPY in DMF displaying a long-lived (~1.4  $\mu$ s) triplet metal-to-ligand charge transfer, <sup>3</sup>MLCT, state.<sup>48</sup> Increasing the doping concentration of RuDCBPY in the UiO-67 material was accompanied by a marked decrease in emission lifetime, which was proposed to be due to homogeneous energy transfer between RuDCBPY centers.<sup>48,49</sup> It was also shown that this same material could be grown onto conductive fluorine-doped tin oxide (FTO) coated glass substrates without changing its excited state properties or dynamics.<sup>49</sup> Therefore, it was postulated that these

Department of Chemistry, Virginia Tech, Blacksburg, VA 24061, USA. E-mail: [ajmorris@vt.edu](mailto:ajmorris@vt.edu)

† Electronic supplementary information (ESI) available: PXRD, TGA, BET, SEM, emission lifetimes, diffuse reflectance, steady state emission, and IPCE/diffuse reflectance overlay. See DOI: [10.1039/c5sc01565k](https://doi.org/10.1039/c5sc01565k)

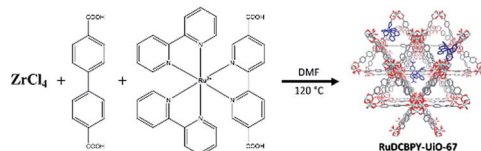


RuDCBPY-doped UiO-67 films could also be grown onto  $\text{TiO}_2$  as a sensitizing material for photovoltaic applications, which is the subject of this report.

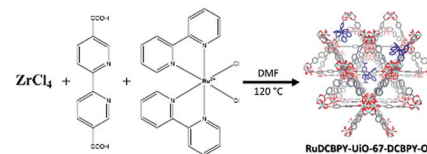
## Results and discussion

A series of zirconium(IV)-based MOFs incorporating ruthenium(II) polypyridyl dyes as ligands, forming the backbone of the material, were explored here as sensitizers for photovoltaic solar cell applications. RuDCBPY–UiO-67 (Scheme 1) and RuDCBPY–UiO-67–DCBPY-X (Schemes 2 and 3) films were solvothermally grown onto  $\text{TiO}_2$ -coated FTO glass as described previously.<sup>49</sup> RuDCBPY–UiO-67–DCBPY-X was prepared by two methods: incubation of  $\text{ZrCl}_4$ , DCBPY, and  $\text{Ru}(\text{bpy})_2\text{Cl}_2$  in DMF and heating at 120 °C for 24 hours to yield RuDCBPY–UiO-67–DCBPY-OP (OP = one pot, Scheme 2), and by post-synthetic modification of a UiO-67–DCBPY film by incubation in an ethanolic solution of  $\text{Ru}(\text{bpy})_2\text{Cl}_2$  to yield RuDCBPY–UiO-67–DCBPY-PS (PS = post synthetic, Scheme 3). The coordination of  $\text{Ru}(\text{bpy})_2$  to the UiO-67–DCBPY was confirmed by diffuse reflectance UV-vis spectroscopy (ESI Fig. S10 and S11†).<sup>50</sup> Presumably, the UiO-67–DCBPY film is stable enough for the RuDCBPY to be prepared *in situ* without perturbation of the morphology of the material. Powder X-ray diffraction patterns (PXRD) of the post-synthetically modified material support this assumption (see Fig. S1 in the ESI†). Lastly, a new Zr(IV)-coordination polymer has also been synthesized and films of the material grown on  $\text{TiO}_2$ -coated FTO, RuDCBPY–ZrMOF– $\text{TiO}_2$  (see ESI† for characterization). The PXRD pattern of the RuDCBPY–ZrMOF powder, though indicative of a crystalline material, was considerably different than that of UiO-67, UiO-67–DCBPY, RuDCBPY–UiO-67, and RuDCBPY–UiO-67–DCBPY (Fig. S1 in ESI†). Additional structural characterization (SEM and PXRD) and the photophysical characteristics of these materials (as well as a number of control materials) are summarized in Table 1 and the ESI.†

In an earlier report, the photophysics of RuDCBPY–UiO-67 thin films grown on FTO were shown to behave similar to RuDCBPY–UiO-67 powders.<sup>49</sup> That is, the long lifetime of the emissive  $^3\text{MLCT}$  state corresponding to RuDCBPY centres incorporated into the backbone of the MOF was found to be sensitive to the degree of RuDCBPY doping within the material. It was purported that this observed increase in the  $^3\text{MLCT}$  decay rate was due to a homogeneous resonance energy transfer reaction between RuDCBPY centres leading to excited state energy migration throughout the material.<sup>48,49</sup> The observed RuDCBPY–RuDCBPY distance dependence on the rate of energy transfer was thought to lie between the Förster and Perrin regimes of donor–acceptor coulombic coupling (*vida infra*).<sup>48</sup>



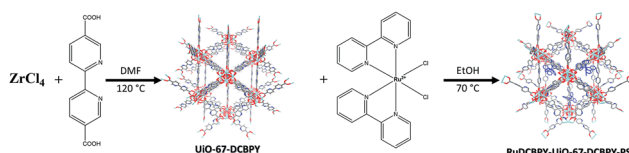
Scheme 1 RuDCBPY–UiO-67.



Scheme 2 RuDCBPY–UiO-67–DCBPY-OP.

Given this, and assuming that the energetics related to the  $\text{Ru}^{3+/2+}$  ground state oxidation of RuDCBPY ( $E_{1/2}(\text{Ru}^{3+/2+}) = 1.50$  V, *vs.* NHE)<sup>51</sup> incorporated in the material is not significantly perturbed relative to RuDCBPY in solution, then these materials present promising sensitizers for photovoltaic applications. The expectation of the invariability of the energetics of RuDCBPY incorporated into the UiO-67 and UiO-67–DCBPY MOFs is based on electrochemical properties of  $\text{Ru}(\text{bpy})_3^{2+}$  encapsulated in zeolite-Y and electrochemical observations of small molecules incorporated into MOFs.<sup>52–56</sup> Indeed, encapsulation of  $\text{Ru}(\text{bpy})_3^{2+}$  by zeolite-Y resulted in negligible perturbation of the  $\text{Ru}^{3+/2+}$  couple.<sup>52</sup> The  $\text{Ru}^{3+/2+}$   $E_{1/2}$  observed in zeolite-Y occurred at  $\sim 1.5$  V (*vs.* NHE, compared to 1.58 V for the same compound in a  $\text{LiBF}_4/\text{CH}_3\text{CN}$  electrolyte solution).<sup>52</sup> Additionally, it has recently been demonstrated that the electrochemical properties of a series of pyrene-based MOF thin films, NU-901 and NU-1000, on FTO do not significantly differ from that observed for the ligand in solution – demonstrating an  $E_{1/2} \sim 1.6$  V (*vs.* NHE) for the reversible pyrene oxidation couple in the MOF compared to  $E_{1/2} \sim 1.54$  V (*vs.* NHE) in solution.<sup>54,56,57</sup>

A moderate photocurrent response was observed for all of the frameworks tested upon front-side illumination of MOF-sensitized  $\text{TiO}_2$  cells constructed with a tetrabutylammonium iodide (TBAI) and iodine based electrolyte in  $\text{CH}_3\text{CN}$  and platinum counter electrode (Fig. 1, 2 and 4). Short circuit current densities ( $J_{\text{SC}}$ ) and open circuit potentials ( $V_{\text{OC}}$ ) were found to range between  $\sim 0.03$  mA cm $^{-2}$  to  $\sim 0.54$  mA cm $^{-2}$  and  $\sim 370$  mV to  $\sim 520$  mV, respectively, leading to maximum observed power conversion efficiencies,  $\eta$ , of 0.125% (Table 2). All of the materials tested showed a significant amount of charge recombination ( $\text{FF}_{\text{avg}} = 0.50$ ); presumably, due to recombination between electrons in the conduction band of  $\text{TiO}_2$  and oxidized redox mediator,  $\text{I}_3^-$ , which may be due to partial occlusion of the pores to  $\text{I}^-$  and/or  $\text{I}_3^-$  diffusion by RuDCBPY. The poor PCEs ( $\eta < 1\%$ ) observed in the electrolyte used here (0.5 M TBAI, 0.05 M  $\text{I}_2$  in  $\text{CH}_3\text{CN}$ ) are not surprising when considering the well-known cation effect on the energetics and kinetics of electron injection into  $\text{TiO}_2$ .<sup>58–61</sup> Indeed, TBA $^+$  has been implicated in deterring electron injection into  $\text{TiO}_2$  relative to other cations.<sup>62</sup> This is purportedly due to a shift in



Scheme 3 RuDCBPY–UiO-67–DCBPY-PS.



Table 1 Summary of diffuse reflectance and emission results<sup>a</sup>

Material (dopant density)	Emission lifetime			
	$\tau''_{\text{obs}}$ (ns)	$\tau'_{\text{obs}}$ (ns)	$E_{\text{MLCT}}^{\text{i}}$ (eV)	$E_{\text{MLCT}}^{\text{s}}$ (eV)
RuDBCPY	DMF	—	880 <sup>b</sup>	462 nm <sup>b</sup> (2.69 eV)
	TiO <sub>2</sub>	25	474	430 nm (2.89 eV)
RuBPY@UiO-67	TiO <sub>2</sub>	23	412	442 nm (2.81 eV)
	TiO <sub>2</sub>	35	388	430 nm (2.89 eV)
RuDCBPY–UiO-67–DCBPY-OP (~20 mm)	FTO	—	327 <sup>c</sup>	449 nm <sup>c</sup> (2.76 eV)
	TiO <sub>2</sub>	4	221	437 nm (2.84 eV)
RuDCBPY–UiO-67–DCBPY-PS (~30 mm)	FTO	—	234	435 nm (2.85 eV)
	TiO <sub>2</sub>	13	143	439 nm (2.83 eV)
RuDCBPY–ZrMOF	FTO	—	133	437 nm (2.84 eV)
	TiO <sub>2</sub>	2	204	437 nm (2.84 eV)
	FTO	16	202	440 nm (2.82 eV)

<sup>a</sup> Errors associated with all values obtained here are  $\pm 5\%$  based on three trials. <sup>b</sup> In DMF according to ref. 48. <sup>c</sup> ref. 49. OP = one pot synthetic method, PS = post-synthetic method. <sup>d</sup>  $E_{\text{MLCT}}^{\text{i}}$  was approximated as the intersection of the diffuse reflectance and emission spectra and  $E_{\text{MLCT}}^{\text{s}}$  was approximated as the maxima of the emission spectra.

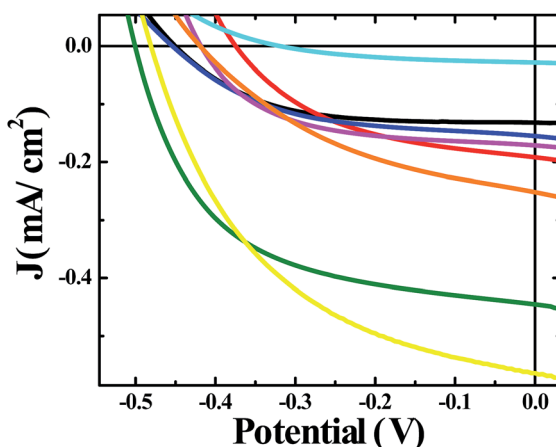


Fig. 1  $J$ – $V$  curves of solar cells constructed with bare unmodified TiO<sub>2</sub> (black), RuDCBPY on TiO<sub>2</sub> (red), undoped UiO-67-TiO<sub>2</sub> (blue), RuBPY@UiO-67-TiO<sub>2</sub> (pink), RuDCBPY–UiO-67–TiO<sub>2</sub> (green), RuDCBPY–UiO-67–DCBPY-OP–TiO<sub>2</sub> (orange), RuDCBPY–UiO-67–DCBPY-PS–TiO<sub>2</sub> (cyan), and RuDCBPY–ZrMOF–TiO<sub>2</sub> (yellow) in a tetrabutylammonium iodide (TBAI) and iodine based electrolyte in CH<sub>3</sub>CN and platinum counter electrode.

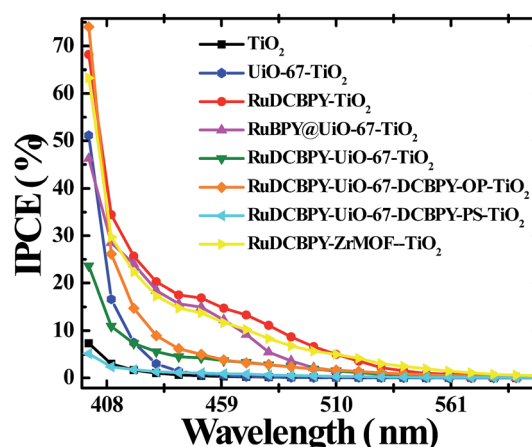


Fig. 2 Incident photon to current conversion efficiency (IPCE) spectra of unmodified TiO<sub>2</sub> (black), RuDCBPY on TiO<sub>2</sub> (red), undoped UiO-67-TiO<sub>2</sub> (blue), RuBPY@UiO-67-TiO<sub>2</sub> (pink), RuDCBPY–UiO-67–TiO<sub>2</sub> (green), RuDCBPY–UiO-67–DCBPY-OP–TiO<sub>2</sub> (orange), RuDCBPY–UiO-67–DCBPY-PS–TiO<sub>2</sub> (cyan), and RuDCBPY–ZrMOF–TiO<sub>2</sub> (yellow) collected in a tetrabutylammonium iodide (TBAI) and iodine based electrolyte in CH<sub>3</sub>CN with a platinum counter electrode.

the TiO<sub>2</sub> energetics possible through the intercalation of small cations such as Li<sup>+</sup>, H<sup>+</sup>, or Na<sup>+</sup> into TiO<sub>2</sub> that is not possible with the larger TBA<sup>+</sup> cation.<sup>58,63</sup>

RuDCBPY–UiO-67–TiO<sub>2</sub> and RuDCBPY–ZrMOF–TiO<sub>2</sub> outperformed (higher  $J_{\text{SC}}$ ,  $V_{\text{OC}}$  and  $\eta$ ) the other constructs tested, including RuDCBPY simply adsorbed on the surface of unmodified TiO<sub>2</sub> and Ru(bpy)<sub>3</sub>Cl<sub>2</sub> diffused into undoped UiO-67 grown on TiO<sub>2</sub>. Additionally, RuDCBPY–UiO-67–DCBPY-PS–TiO<sub>2</sub> performed comparatively worse than the unmodified TiO<sub>2</sub> control. This is evidence that synthetic procedure has a direct impact on observed photophysical properties. Since all of the MOFs tested contain RuDCBPY light-active centres, the source of varied solar cell performance is most likely not molecular in origin but rather due to the 3D orientation and localization of

these centres within the MOFs. Below, we will discuss such structure dependent effects in the context of the photophysical processes involved in the explored MOFSCs.

The MOFSCs reported here differ significantly from conventional DSC in that the sensitizing “dyes” are expected to be spatially distributed on the TiO<sub>2</sub> surface and above the TiO<sub>2</sub> throughout the backbone of the MOF crystalline matrix (Fig. 3). In this geometry, there are at least three processes accounting for the observed photocurrent and excited state quenching dynamics upon illumination of the MOF (summarized in Fig. 4): (1) excitation of the UiO-67 or UiO-67-DCBPY followed by charge separation and electron injection into TiO<sub>2</sub>, (2) excitation of RuDCBPY ligands within the energy diffusion distance that through energy hopping/migration and/or direct



interactions results in electron injection into  $\text{TiO}_2$ , and (3) energy hopping/migration between RuDCBPY centres within the bulk of the MOF beyond the energy hopping diffusion length from the MOF- $\text{TiO}_2$  interface.

### (1) Charge separation between the $\text{UiO-67}$ MOF backbone and $\text{TiO}_2$

It is possible that illumination of undoped  $\text{UiO-67}$  with broadband light results in BPDC-localized reactive singlet and/or triplet excited state(s) which undergo charge separation at the MOF- $\text{TiO}_2$  interface. This is energetically plausible considering the energy gap between the highest occupied molecular orbitals (HOMOs) and lowest unoccupied molecular orbitals (LUMOs) of  $\text{UiO-67}$  at  $\sim 3.6$  eV ( $\sim 340$  nm absorption band edge) reported previously for  $\text{UiO-67}$ , which agrees well with our observations (not shown).<sup>64</sup> Computational evidence suggest the LUMOs of the  $\text{UiO}$ -type frameworks are largely comprised of Zr d-states whereas the ligand H s-, C s-, and O p-states contribute to the HOMOs.<sup>65</sup> In addition, transient diffuse reflectance measurements performed on the  $\text{UiO-66}$  MOF, a benzene-1,4-dicarboxylate (BDC) analogue of  $\text{UiO-67}$ , indicate that the transients observed upon 355 nm excitation are sensitive to  $\text{O}_2$ , a known quencher of triplet states.<sup>66</sup> This is suggestive of formation of a BDC-localized triplet, which presents a broad and diffuse transient spectra between 350 nm and 800 nm.<sup>35</sup> Charge separation between the  $\text{UiO-67}$  backbone and  $\text{TiO}_2$  is further supported here by the observation of modest photocurrent upon one sun illumination of undoped  $\text{UiO-67}$  grown on  $\text{TiO}_2$  in addition to the slightly improved performance over unmodified  $\text{TiO}_2$  (Table 2, Fig. 1 and 2). As evident from the results shown in Table 2, the contribution of the  $\text{UiO-67}$  to the total photocurrent is minimal. Therefore, the dynamics of electron injection into  $\text{TiO}_2$  by the  $\text{UiO-67}$  was not explored further.

### (2) Charge separation between RuDCBPY at or within the energy hopping distance from the MOF- $\text{TiO}_2$ interface and $\text{TiO}_2$

Upon excitation, the observed emission lifetime decays of the Ru-MOF/ $\text{TiO}_2$  photoanodes probed here displayed non-exponential kinetics. The decays were best fit to a bi-exponential decay model and the results are summarized in Table 1. The bi-exponential fits indicate the presence of a slow 100–300 ns

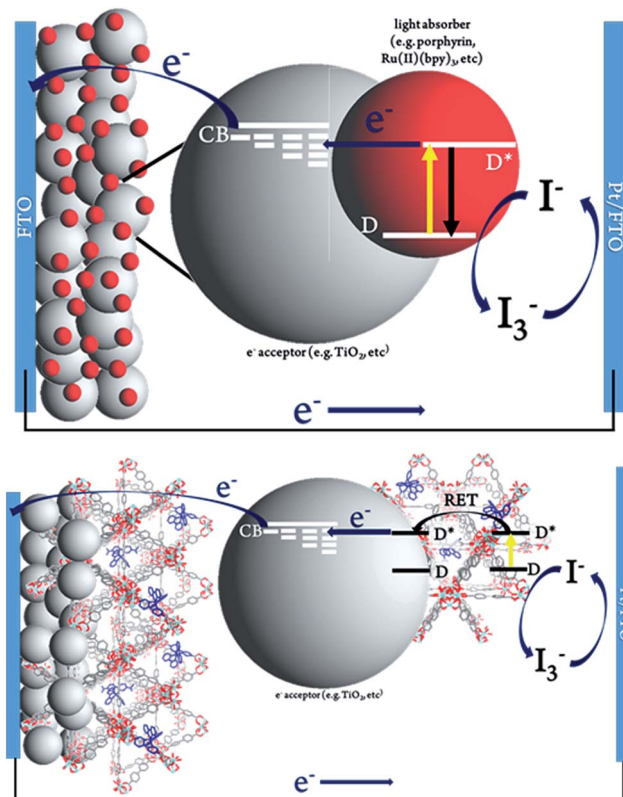


Fig. 3 Schematic representation of (top) conventional dye-sensitized solar cell and (bottom) Ru-MOF sensitized solar cells, MOFSCs.

phase and a fast 4 ns to 30 ns phase. The magnitude of the slow lifetime component of the decays are consistent with the magnitude of the exponential lifetime decays in the absence of  $\text{TiO}_2$ . Time-resolved emission decays of  $\text{Ru}(\text{bpy})_2(4,4'\text{-DCBPY})$ ,  $4,4'\text{-DCBPY} = 2,2'\text{-bipyridyl-4,4'-dicarboxylic acid}$ , on  $\text{TiO}_2$  often display complex kinetics with lifetimes in the range of 1 ns to 2  $\mu\text{s}$ .<sup>67,68</sup> By analogy to these reports and the results obtained here, the fast component of the emission decays ( $\tau''_{\text{obs}}$ ) is ascribed to the quenching of the RuDCBPY excited states at or within the energy hopping distance ( $R_{\text{hop}}$ ) from the MOF- $\text{TiO}_2$  interface by electron injection from RuDCBPY into  $\text{TiO}_2$ . The long lifetime component ( $\tau'_{\text{obs}}$ ), however, is attributed to homogeneous RET occurring within the MOF bulk at distances from the MOF- $\text{TiO}_2$  junction greater than  $R_{\text{hop}}$  (*vide infra*).

Table 2 Summary of  $J$ - $V$  results<sup>a</sup>

	$J_{\text{SC}}$ (mA cm $^{-2}$ )	$V_{\text{OC}}$ (V)	FF	$\eta$ (%)
$\text{TiO}_2$	$-0.132 \pm 0.001$			$0.034 \pm 0.011$
RuDCBPY- $\text{TiO}_2$	$-0.203 \pm 0.051$	$-0.451 \pm 0.010$	$0.57 \pm 0.05$	$0.077 \pm 0.010$
$\text{UiO-67-DCBPY-TiO}_2$	$-0.180 \pm 0.003$	$-0.364 \pm 0.047$	$0.46 \pm 0.01$	$0.049 \pm 0.005$
RuBPY@ $\text{UiO-67-TiO}_2$	$-0.175 \pm 0.068$	$-0.471 \pm 0.036$	$0.59 \pm 0.03$	$0.045 \pm 0.015$
RuDCBPY- $\text{UiO-67-TiO}_2$	$-0.446 \pm 0.097$	$-0.455 \pm 0.072$	$0.57 \pm 0.06$	$0.123 \pm 0.021$
RuDCBPY- $\text{UiO-67-DCBPY-OP-TiO}_2$	$-0.251 \pm 0.025$	$-0.480 \pm 0.019$	$0.55 \pm 0.04$	$0.046 \pm 0.005$
RuDCBPY- $\text{UiO-67-DCBPY-PS-TiO}_2$	$-0.028 \pm 0.005$	$-0.420 \pm 0.026$	$0.44 \pm 0.06$	$0.004 \pm 0.001$
RuDCBPY-ZrMOF- $\text{TiO}_2$	$-0.564 \pm 0.129$	$-0.324 \pm 0.035$	$0.41 \pm 0.05$	$0.125 \pm 0.038$

<sup>a</sup> Average values and errors shown are based on at least 3 trials.



The slow component of the emission decay rate is comprised of the natural lifetime of RuDCBPY, in other words the sum of the radiative and non-radiative decay rate constants in the absence of intermolecular interactions ( $k_r + k_{nr}$ ), as well as a quenching rate constant corresponding to the rate of energy migration,  $k_{hop}$ , according to

$$(\tau'_{obs})^{-1} = k_r + k_{nr} + k_{hop} \quad (1)$$

The second, fast lifetime component in the emission decays,  $(\tau''_{obs})^{-1}$ , should have contributions from the natural  $^3$ MLCT decay rate of RuDCBPY,  $k_r + k_{nr}$ , plus contributions from resonance energy transfer and migration,  $k_{hop}$ , and an additional electron transfer/injection term,  $k_{inj}$ .

$$(\tau''_{obs})^{-1} = k_r + k_{nr} + k_{hop} + k_{inj} \quad (2)$$

The values from eqn (2) for  $k_{inj}$  were obtained by assuming the sum of  $k_r$ ,  $k_{nr}$ , and  $k_{hop}$  were approximately equal to  $(\tau'_{obs})^{-1}$  and are included in Table 3.

The electron injection efficiency,  $\Phi_{inj}$ , at the  $TiO_2$ -MOF interface is then defined as the product of  $\tau''_{obs}$  and  $k_{inj}$ :

$$\Phi_{inj} = \tau''_{obs} k_{inj} \quad (3)$$

The magnitudes of  $k_{inj}$  and  $\Phi_{inj}$  presented in Table 3 are indicative of strong coupling between RuDCBPY and  $TiO_2$ .

### (3) Energy transfer/hopping within the bulk of the MOF beyond the energy hopping diffusion length from the MOF- $TiO_2$ interface

Illumination of RuDCBPY centres found throughout the bulk of the material result in formation of a  $^1$ MLCT excited state

which quickly undergoes intersystem crossing to generate an emissive  $^3$ MLCT excited state. It has been observed that in RuDCBPY-doped  $UiO$ -67 powders and films, the emission lifetime of the  $^3$ MLCT excited state decreases dramatically as the number of RuDCBPY centres is increased within the material.<sup>48,49</sup> It was argued that the origin of the quenching of the long lifetime component of the emission decay is homogeneous resonance energy transfer between RuDCBPY centres within the material. The aforementioned slow component of the bi-exponential emission lifetime decay is attributed to this process based on the similarities of their magnitudes with the magnitude of the lifetime obtained previously for RuDCBPY- $UiO$ -67.<sup>48,49</sup> From eqn (1),  $k_{hop}$  was calculated to be between  $1.9 \times 10^6 \text{ s}^{-1}$  and  $6.3 \times 10^6 \text{ s}^{-1}$  for the Ru-MOF/ $TiO_2$  photoanodes explored here (where  $k_r + k_{nr}$  is taken here to be  $7.14 \times 10^5 \text{ s}^{-1}$  for dilute concentrations of RuDCBPY in  $UiO$ -67).

The average hopping distance,  $R_{hop}$ , is related to  $k_{hop}$  according to eqn (4),

$$k_{hop} = \frac{m D_{RET}}{R_{hop}^2} \quad (4)$$

where  $m$  is a dimensional factor ( $m = 6$  for three dimensional systems,  $m = 4$  for two dimensional systems, and  $m = 2$  for one dimensional energy hopping) and  $D_{RET}$  is the diffusion coefficient for energy migration (taken here to be  $2 \times 10^{-6} \text{ cm}^2 \text{ s}^{-1}$  based on the triplet exciton diffusion rate of crystalline  $Ru(bpy)_3$  salts).<sup>69</sup> The  $R_{hop}$  values corresponding to three dimensional energy transfer throughout the film were 254 Å for RuDCBPY- $UiO$ -67, 177 Å for RuDCBPY- $UiO$ -67-DCBPY- $TiO_2$ -OP, 138 Å for RuDCBPY- $UiO$ -67-DCBPY- $TiO_2$ -PS, and 169 Å for RuDCBPY-ZrMOF.

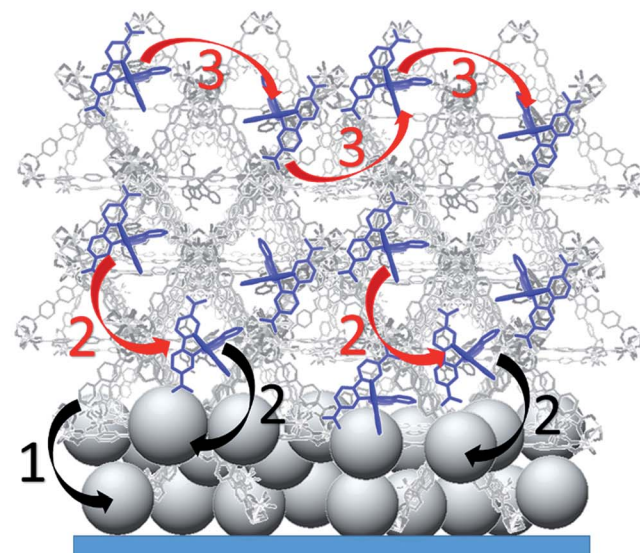
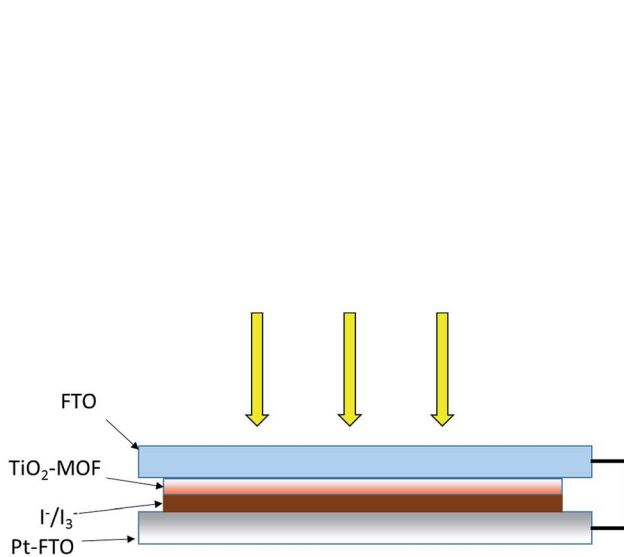


Fig. 4 (Left) Front-side solar cell sandwich arrangement used for the photovoltaic cells prepared here. (Right) General scheme depicting the potential processes contributing to the observed photocurrent for the RuDCBPY-MOF modified  $TiO_2$  films. The black arrows indicate charge separation steps whereas the red arrows are indicative of energy transfer/hopping between RuDCBPY centers within the MOF. (1) Charge separation between the BPDC or DCBPY MOF ligands and  $TiO_2$ . (2) Charge separation between RuDCBPY centers at or within the energy hopping diffusion length from the MOF/ $TiO_2$  interface and the  $TiO_2$ . (3) Non-directional energy transfer/hopping between RuDCBPY centers within the MOF.



Table 3 Summary of energy and electron transfer parameters obtained from photophysical data

	$k_{\text{hop}} (\times 10^6 \text{ s}^{-1})$	$k_{\text{inj}} (\times 10^7 \text{ s}^{-1})$	$\Phi_{\text{RET}}$	$\Phi_{\text{inj}}$	$r (\text{\AA})$	$R_{\text{hop}} (3\text{D}, \text{\AA})$	$R_{\text{hop}} (2\text{D}, \text{\AA})$	$R_{\text{hop}} (1\text{D}, \text{\AA})$
RuDCBPY–UiO-67–TiO <sub>2</sub>	1.86	2.59	0.72	0.91	24	254	207	147
RuDCBPY–UiO-67–DCBPY–TiO <sub>2</sub> –OP	3.81	24.5	0.84	0.98	19	177	145	102
RuDCBPY–UiO-67–DCBPY–TiO <sub>2</sub> –PS	6.28	6.99	0.89	0.91	16	138	113	80
RuDCBPY–ZrMOF–TiO <sub>2</sub>	4.19	49.5	0.85	0.99	19	169	138	98

The average RuDCBPY intermolecular distances,  $r$ , were calculated from the value of  $R_{\text{hop}}$  and the energy transfer efficiency,  $\Phi_{\text{RET}}$ , according to the relationship:

$$\Phi_{\text{RET}} = 1 - \frac{\tau'_{\text{obs}}}{\tau_0} = \frac{1}{1 + (r/R_{\text{hop}})^3} \quad (5)$$

where  $\tau_0$  is the <sup>3</sup>MLCT lifetime of RuDCBPY in the UiO-67 MOF in the absence of quenching ( $\sim 1.4 \mu\text{s}$ ).<sup>48</sup> An average distance of 20 Å is approximated between interacting RuDCBPY centres in all RuDCBPY-containing MOFs reported here, which agrees well with those results obtained previously for RuDCBPY–UiO-67 films grown on FTO ( $r \sim 22 \text{ \AA}$ ).<sup>49</sup> Based on the UiO-67 morphology which includes two types of pores, a tetrahedral cavity  $\sim 12 \text{ \AA}$  in diameter as well as an octahedral cavity  $\sim 23 \text{ \AA}$  in diameter, the  $r$  values obtained from eqn (5) are physically reasonable considering the possible positions of the dye occupation within the MOF pores.<sup>70,71</sup>

At low doping concentrations and large RuDCBPY intermolecular separation within the MOF, the distance dependence of the energy transfer was found to lie between the very-weak and weak coupling regime based on an Inokuti–Hirayama analysis of the lifetime decays.<sup>48,49,72</sup> That is, the rate of RET was proposed to be proportional to an  $r^{-4}$  intermolecular distance dependence. The Inokuti–Hirayama equation, however, assumes that the interactions between energy donors and acceptors occur over three-dimensions.<sup>72</sup> Recent evidence suggests that, in the case of post-synthetically doped materials, the dimensionality of energy transfer occurring between RuDCBPY centres is dependent on the doping concentration.<sup>50</sup> For that reason,  $R_{\text{hop}}$ , has also been calculated for two dimensional, and one dimensional RET (Table 3). Alternatively, intermolecular energy migration according to the Dexter mechanism has been observed between ruthenium centres in a variety of MOF structures.<sup>41–45</sup> For example, Meyer, *et al.* have reported a MOF consisting of Ru(II)(2,2'-bipyridyl-4,4'-dicarboxylic acid)<sub>2</sub>(2,2'-bipyridine)[PF<sub>6</sub>]<sub>2</sub> ligands and Zn(II) carboxylate nodes displaying Ru<sup>+</sup>–Ru energy migration up to 40 Å by the Dexter mechanism.<sup>42</sup>

The results in Table 3 suggest a large degree of coupling between interacting RuDCBPY centres such that energy hopping/migration occurs over distances up to 15 nm on average. This distance is, however, considerably smaller than the average thickness of the films grown solvothermally ( $\sim 10 \mu\text{m}$  based on SEM, Fig. S7†).<sup>49</sup> From theoretical considerations, it has been shown that the electron injection yield is expected to decrease as a function of increasing number of energy “hopping” units in multimeric light harvesting arrays.<sup>73</sup>

Therefore, the energy “harvested” at RuDCBPY-centres in the UiO-67 and UiO-67–DCBPY bulk at distances further than 15 nm from the TiO<sub>2</sub>–MOF interface is likely lost to thermalization.<sup>74</sup>

Although the differences between resonance energy transfer, electron injection efficiencies, and power conversion efficiencies for the RuDCBPY containing MOFs explored are not very large, a few observations of interest are pointed out. In terms of resonance energy transfer, it seems that the RuDCBPY–UiO-67–DCBPY–PS–TiO<sub>2</sub> displayed the largest degree of coupling between RuDCBPY centres and interacting pairs (based on the magnitude of  $k_{\text{hop}}$ ) followed by RuDCBPY–ZrMOF–TiO<sub>2</sub>, RuDCBPY–UiO-67–DCBPY–OP–TiO<sub>2</sub>, and then RuDCBPY–UiO-67–TiO<sub>2</sub>. This could be due to the nature of the post-synthetic preparative method. It has been shown by confocal fluorescence microscopy that denser populations of RuDCBPY centres form along the edges and vertices of the UiO-67–DCBPY surface closest to the MOF–solution interface regardless of the degree of doping.<sup>50</sup> It was purported that the non-uniform distribution of RuDCBPY doping in the framework by the post-synthetic method was likely due to diffusional limitations of the Ru(bpy)<sub>2</sub>Cl<sub>2</sub> imposed by the MOF (either steric or thermodynamic in nature) inhibiting penetration of RuDCBPY into the bulk of the crystalline material. This was supported by recent evidence obtained by fluorescence microscopy depicting the loading of a IRMOF-10 MOF with Ru(bpy)<sub>2</sub>(dpbpy), dpbpy = 4,4'-diphosphonate-2,2'-bipyridine, by slow diffusion in a CH<sub>3</sub>CN solution.<sup>39</sup>

The poor PCE of the RuDCBPY–UiO-67–DCBPY–PS–TiO<sub>2</sub> material is then a direct consequence of the nature of the post-synthetic preparative method if the formation of RuDCBPY centres throughout the UiO-67–DCBPY film saturates the outer layers near the MOF–solution interface yet only sparingly populate the MOF–bulk and, in particular, the MOF–TiO<sub>2</sub> interface. Significant differences between the diffuse reflectance and IPCE of RuDCBPY–UiO-67–DCBPY–TiO<sub>2</sub>–PS are evident when overlain (Fig. S20†). Specifically, the differences present are indicative of reduced contribution of the RuDCBPY to the total photocurrent. These observations are attributed to thermalization of those RuDCBPY excited states generated outside of the  $R_{\text{hop}}$  distance away from the MOF–TiO<sub>2</sub> interface. Similarly, the dramatically reduced  $J_{\text{SC}}$  and  $V_{\text{OC}}$  values relative to the other Ru-MOFSCs might be explained by occlusion of the UiO-67–DCBPY pores by RuDCBPY formation on the outer layers of the films which may obstruct diffusion of I<sub>3</sub><sup>–</sup> into the MOF restricting regeneration of RuDCBPY after electron injection into TiO<sub>2</sub>. It should be noted that accessibility of I<sup>–</sup> to oxidized



RuDCBPY sites and effusion of  $I_3^-$  out of the MOF may also be hindered in the RuDCBPY–UiO-67 and RuDCBPY–UiO-67-OP films. However, the presumed random distribution of the RuDCBPY ligands throughout the volume of the MOF relative to that proposed for RuDCBPY–UiO-67-PS likely increases the number of available diffusion pathways for  $I^-$  and  $I_3^-$  in, out, and through the films relative to RuDCBPY–UiO-67-PS. These observations may point to the importance of the role of interfacial RuDCBPY at the MOF– $TiO_2$  boundary. It is likely that “one-pot” methods of preparing the MOFSCs using the pre-formed dye, *i.e.* RuDCBPY–UiO-67 and RuDCBPY–ZrMOF, result in larger concentrations of dye at the surface as well as a more uniform distribution of dye throughout the bulk of the framework suggesting a concentration and spatial distribution effect on the efficacy of the MOFSC.

## Conclusion

To summarize, a series of RuDCBPY containing zirconium(IV)-based metal–organic frameworks were grown as thin films on  $TiO_2$  as sensitizing materials for photovoltaic applications. It was found that the mechanisms of excited state energy migration and electron transfer into  $TiO_2$  seem to be similar between materials. That is, upon generation of the RuDCBPY excited state, the energy of the excited state migrates through the film *via* RuDCBPY interacting pairs that are separated, on average, by  $\sim 20$  Å. The values obtained for the rate of energy migration,  $k_{hop}$ , indicate that RuDCBPY centres located at the MOF– $TiO_2$  interface are sensitized either directly upon absorption of the incident irradiation or indirectly *via* resonance energy transfer processes initiated up to 15 nm away from the interface. Additionally, it seems that the choice of the preparative method of photoactive MOFs has a large effect on the power conversion efficiency of the MOFSC. Although the efficiencies of the cells prepared here are less than 1%, the MOFSCs outperformed a monolayer of the same dye on the surface of  $TiO_2$  and, therefore, present a promising platform for photovoltaic applications.

## Experimental

The chemicals and solvents were obtained from either Sigma-Aldrich or Fisher Scientific and used as received without further purification unless otherwise noted below.

### (1) Synthesis of $Ru(2,2'$ -bipyridine)<sub>2</sub>(5,5'-dicarboxy-2,2'-bipyridine)Cl<sub>2</sub>, RuDCBPY

The synthesis of RuDCBPY has been described previously and was carried out accordingly.<sup>51</sup> Ru(bpy)<sub>2</sub>Cl<sub>2</sub> (160 mg, Alfa Aesar, 97%) and DCBPY (100 mg, Ark Pharm, Inc, >95%) were dissolved in 20 mL of an ethanol–basic water mix (1 : 1 v/v) and refluxed under  $N_2$  overnight. The solution was cooled to room temperature and the solvent removed by rotary evaporation and recrystallized from MeOH–diethyl ether.

### (2) Synthesis of UiO-67-DCBPY

The synthetic procedure used to prepare UiO-67-DCBPY films was similar to a previously reported procedure for UiO-67.<sup>48,49,75</sup> In a typical synthesis, 0.13 g of ZrCl<sub>4</sub> (98%), and 0.14 g of DCBPY (95%) were suspended in 20 mL of anhydrous DMF (>99%) and sonicated in a 6 dram vial for five minutes. A clean FTO substrate was then introduced to the mixture. The vial was then sealed and heated at 120 °C for 12 hours after which the film was cooled to room temperature, rinsed with DMF, and dried. MOF films were grown on  $TiO_2$ –FTO substrates in the same manner just described.

### (3) Preparation of RuDCBPY–UiO-67

Films of RuDCBPY–UiO-67 were prepared solvothermally according to a previously reported method similar to what was described above for UiO-67-DCBPY.<sup>49</sup> Briefly, 0.13 g of ZrCl<sub>4</sub>, 0.14 g of DCBPY and 0.03 g of RuDCBPY were mixed in a 6 dram vial containing 20 mL DMF and a clean FTO substrate, sealed, and heated to 120 °C for 12 hours. The films were then rinsed thoroughly with DMF and dried. MOF films were grown on  $TiO_2$ –FTO substrates in the same manner just described.

### (4) Preparation of RuDCBPY–UiO-67–DCBPY (one pot method)

RuDCBPY–UiO-67–DCBPY-OP films were grown on FTO and  $TiO_2$ –FTO by mixing 0.13 g of ZrCl<sub>4</sub>, 0.14 g DCBPY, and 0.02 g Ru(bpy)<sub>2</sub>Cl<sub>2</sub> (Alfa Aesar, 97%) in a 6 dram vial containing 20 mL of dry DMF. The mixture was sonicated for five minutes and the FTO substrate introduced. The vial was then sealed and heated to 120 °C for 12 hours. The film was then cooled to room temperature, rinsed thoroughly with DMF and dried.

### (5) Preparation of RuDCBPY–UiO-67–DCBPY (post synthetic method)

Fresh UiO-67-DCBPY films were incubated in ethanolic solutions containing 0.02 g Ru(bpy)<sub>2</sub>Cl<sub>2</sub> (Alfa Aesar, 97%) and allowed to soak for 3 days before heating at 70 °C for 3 additional days. Once cooled to room temperature, the resulting RuDCBPY–UiO-67–DCBPY films were rinsed thoroughly with DMF and deionized water.

### (6) Preparation of RuDCBPY–ZrMOF powders and films

RuDCBPY–ZrMOF films were prepared by mixing RuDCBPY (0.03 g) and 0.14 g ZrCl<sub>4</sub> in a 6 dram vial containing 10 mL dry DMF, sonating for 5 minutes and heating at 120 °C for 12 hours after introducing an FTO or  $TiO_2$ –FTO substrate. Powders were similarly prepared except instead of the components being mixed in 10 mL DMF, they were mixed in 10 mL of a DMF/formic acid mixture (1 : 1 v/v).

### (7) Preparation of DSCs

Anatase  $TiO_2$  (Ti Nanoxide, Solaronix, 15–20 nm particle size) was doctor bladed onto clean FTO glass substrates and sintered at 450 °C for thirty minutes. The  $TiO_2$  coated FTO substrates



were then placed in a 6 dram vial under the same conditions described above for the MOFSC materials. The sealed vial containing the reaction mixture was heated at 120 °C for 12 hours after which the product films were then cooled, and rinsed with DMF and acetone.

The MOFSC photoanode was covered with a Pt sputter coated FTO glass slide and held in place using Surlyn (Dupont, 75 micron thickness). An acetonitrile electrolyte solution was prepared containing 0.5 M tetrabutylammonium iodide and 0.05 M iodine for the MOFSC measurements.

### (8) Characterization

*J-V* data was collected using either a Basi Epsilon or a Pine WaveNOW potentiostat. Samples were illuminated using a Newport LCS-100 Solar Simulator equipped with an AM1.5G air mass filter calibrated to 1 sun output. IPCE curves were obtained by measuring the photocurrent generated by illumination of samples using a PTI 75 W Xe arc lamp passed through an OBB 200 mm meter Czerny-turner monochromator and normalizing the observed photocurrent by the output photon density of the arc lamp.

## Acknowledgements

This material is based upon work supported by the U.S. Department of Energy, Office of Science, Office of Basic Energy Sciences under Award Number DE-SC0012446.

## Notes and references

- 1 Z. Dou, J. Yu, Y. Cui, Y. Yang, Z. Wang, D. Yang and G. Qian, *J. Am. Chem. Soc.*, 2014, **136**, 5527–5530.
- 2 D. Y. Lee, C. Y. Shin, S. J. Yoon, H. Y. Lee, W. Lee, N. K. Shrestha, J. K. Lee and S.-H. Han, *Sci. Rep.*, 2014, **4**, 3930.
- 3 H. Li, M. Eddaoudi, T. L. Groy and O. M. Yaghi, *J. Am. Chem. Soc.*, 1998, **120**, 8571–8572.
- 4 J.-L. Wang, C. Wang and W. Lin, *ACS Catal.*, 2012, **2**, 2630–2640.
- 5 M. Pramanik, A. K. Patra and A. Bhaumik, *Dalton Trans.*, 2013, **42**, 5140–5149.
- 6 C. G. Silva, A. Corma and H. Garcia, *J. Mater. Chem.*, 2010, **20**, 3141–3156.
- 7 G.-Y. Wang, C. Song, D.-M. Kong, W.-J. Ruan, Z. Chang and Y. Li, *J. Mater. Chem. A*, 2014, **2**, 2213–2220.
- 8 X. Z. Song, S. Y. Song, S. N. Zhao, Z. M. Hao, M. Zhu, X. Meng and H. J. Zhang, *Dalton Trans.*, 2013, **42**, 8183–8187.
- 9 S. Zhou, Z.-G. Kong, Q.-W. Wang and C.-B. Li, *Inorg. Chem. Commun.*, 2012, **25**, 1–4.
- 10 M. C. So, G. P. Wiederrecht, J. E. Mondloch, J. T. Hupp and O. K. Farha, *Chem. Commun.*, 2015, 3501–3510.
- 11 A. Fateeva, P. A. Chater, C. P. Ireland, A. A. Tahir, Y. Z. Khimyak, P. V. Wiper, J. R. Darwent and M. J. Rosseinsky, *Angew. Chem., Int. Ed.*, 2012, **51**, 7440–7444.
- 12 J.-J. Wang, T.-L. Hu and X.-H. Bu, *CrystEngComm*, 2011, **13**, 5152–5161.
- 13 T. Zhang and W. Lin, *Chem. Soc. Rev.*, 2014, **43**, 5982–5993.
- 14 R. W. Larsen, J. Miksovska, R. L. Musselman and L. Wojtas, *J. Phys. Chem. A*, 2011, **115**, 11519–11524.
- 15 C. L. Whittington, L. Wojtas and R. W. Larsen, *Inorg. Chem.*, 2014, **53**, 160–166.
- 16 M. D. Allendorf, C. A. Bauer, R. K. Bhakta and R. J. T. Houk, *Chem. Soc. Rev.*, 2009, **38**, 1330–1352.
- 17 C. A. Bauer, S. C. Jones, T. L. Kinnibrugh, P. Tongwa, R. A. Farrell, A. Vakil, T. V. Timofeeva, V. N. Khrustalev and M. D. Allendorf, *Dalton Trans.*, 2014, **43**, 2925–2935.
- 18 S. T. Meek, R. J. T. Houk, F. P. Doty and M. D. Allendorf, *Nanoscale Luminescent Materials*, 2010, vol. 28, pp. 137–143.
- 19 J. J. Perry, C. A. Bauer and M. D. Allendorf, in *Metal-Organic Frameworks: Applications from Catalysis to Gas Storage*, ed. D. Farrusseng, 2011, pp. 269–308.
- 20 Y. J. Cui, B. L. Chen and G. D. Qian, *Coord. Chem. Rev.*, 2014, **273**, 76–86.
- 21 Y. J. Cui, Y. F. Yue, G. D. Qian and B. L. Chen, *Chem. Rev.*, 2012, **112**, 1126–1162.
- 22 J. J. Shen, M. X. Li, Z. X. Wang, C. Y. Duan, S. R. Zhu and X. He, *Cryst. Growth Des.*, 2014, **14**, 2818–2830.
- 23 J. Rocha, L. D. Carlos, F. A. A. Paz and D. Ananias, *Chem. Soc. Rev.*, 2011, **40**, 926–940.
- 24 D. Y. Lee, E. K. Kim, C. Y. Shin, D. V. Shinde, W. Lee, N. K. Shrestha, J. K. Lee and S. H. Han, *RSC Adv.*, 2014, **4**, 12037–12042.
- 25 D. Y. Lee, C. Y. Shin, S. J. Yoon, H. Y. Lee, W. Lee, N. K. Shrestha, J. K. Lee and S. H. Han, *Sci. Rep.*, 2014, **4**, 3930.
- 26 D. Y. Lee, D. V. Shinde, S. J. Yoon, K. N. Cho, W. Lee, N. K. Shrestha and S. H. Han, *J. Phys. Chem. C*, 2014, **118**, 16328–16334.
- 27 K. Leong, M. E. Foster, B. M. Wong, E. D. Spoerke, D. van Gough, J. C. Deaton and M. D. Allendorf, *J. Mater. Chem. A*, 2014, **2**, 3389–3398.
- 28 J. S. Li, X. J. Sang, W. L. Chen, L. C. Zhang, Z. M. Su, C. Qin and E. B. Wang, *Inorg. Chem. Commun.*, 2013, **38**, 78–82.
- 29 B. Li, X. Chen, F. Yu, W. J. Yu, T. L. Zhang and D. Sun, *Cryst. Growth Des.*, 2014, **14**, 410–413.
- 30 H. A. Lopez, A. Dhakshinamoorthy, B. Ferrer, P. Atienzar, M. Alvaro and H. Garcia, *J. Phys. Chem. C*, 2011, **115**, 22200–22206.
- 31 V. Stavila, A. A. Talin and M. D. Allendorf, *Chem. Soc. Rev.*, 2014, **43**, 5994–6010.
- 32 F. Xamena, A. Corma and H. Garcia, *J. Phys. Chem. C*, 2007, **111**, 80–85.
- 33 F. Bella, R. Bongiovanni, R. S. Kumar, M. A. Kulandainathan and A. M. Stephan, *J. Mater. Chem. A*, 2013, **1**, 9033–9036.
- 34 M. Alvaro, E. Carbonell, B. Ferrer, F. X. L. I. Xamena and H. Garcia, *Chem.-Eur. J.*, 2007, **13**, 5106–5112.
- 35 M. de Miguel, F. Ragon, T. Devic, C. Serre, P. Horcajada and H. Garcia, *ChemPhysChem*, 2012, **13**, 3651–3654.
- 36 J. X. Liu, W. C. Zhou, J. X. Liu, I. Howard, G. Kilibarda, S. Schlabach, D. Coupry, M. Addicoat, S. Yoneda, Y. Tsutsui, T. Sakurai, S. Seki, Z. B. Wang, P. Lindemann, E. Redel, T. Heine and C. Woll, *Angew. Chem., Int. Ed.*, 2015, **54**, 7441–7445.



37 L.-L. Li and E. W.-G. Diau, *Chem. Soc. Rev.*, 2013, **42**, 291–304.

38 U. Mehmood, S. Rahman, K. Harrabi, I. A. Hussein and B. V. S. Reddy, *Adv. Mater. Sci. Eng.*, 2014, **2014**, 1–12.

39 Y. Tang, W. He, Y. Lu, J. Fielden, X. Xiang and D. Yan, *J. Phys. Chem. C*, 2014, **118**, 25365–25373.

40 W. M. Campbell, K. W. Jolley, P. Wagner, K. Wagner, P. J. Walsh, K. C. Gordon, L. Schmidt-Mende, M. K. Nazeeruddin, Q. Wang, M. Grätzel and D. L. Officer, *J. Phys. Chem. C*, 2007, **111**, 11760–11762.

41 C. A. Kent, D. Liu, T. J. Meyer and W. Lin, *J. Am. Chem. Soc.*, 2012, **134**, 3991–3994.

42 C. A. Kent, B. P. Mehl, L. Q. Ma, J. M. Papanikolas, T. J. Meyer and W. B. Lin, *J. Am. Chem. Soc.*, 2010, **132**, 12767–12769.

43 C. A. Kent, D. M. Liu, L. Q. Ma, J. M. Papanikolas, T. J. Meyer and W. B. Lin, *J. Am. Chem. Soc.*, 2011, **133**, 12940–12943.

44 C. A. Kent, D. M. Liu, A. Ito, T. Zhang, M. K. Brennaman, T. J. Meyer and W. B. Lin, *J. Mater. Chem. A*, 2013, **1**, 14982–14989.

45 J. X. Lin, X. Q. Hu, P. Zhang, A. van Rynbach, D. N. Beratan, C. A. Kent, B. P. Mehl, J. M. Papanikolas, T. J. Meyer, W. B. Lin, S. S. Skourtis and M. Constantinou, *J. Phys. Chem. C*, 2013, **117**, 22250–22259.

46 R. W. Larsen and L. Wojtas, *J. Mater. Chem. A*, 2013, **1**, 14133–14139.

47 R. W. Larsen and L. Wojtas, *J. Phys. Chem. A*, 2012, **116**, 7830–7835.

48 W. A. Maza and A. J. Morris, *J. Phys. Chem. C*, 2014, **118**, 8803–8817.

49 W. A. Maza, S. R. Ahrenholtz, C. C. Epley, C. S. Day and A. J. Morris, *J. Phys. Chem. C*, 2014, **118**, 14200–14210.

50 W. A. Maza, R. Padilla and A. J. Morris, *J. Am. Chem. Soc.*, 2015, **137**, 8161–8168.

51 P. H. Xie, Y. J. Hou, B. W. Zhang, Y. Cao, F. Wu, W. J. Tian and J. C. Shen, *J. Chem. Soc., Dalton Trans.*, 1999, 4217–4221.

52 E. Briot, F. Bedioui and K. J. Balkus, *J. Electroanal. Chem.*, 1998, **454**, 83–89.

53 S. R. Ahrenholtz, C. C. Epley and A. J. Morris, *J. Am. Chem. Soc.*, 2014, **136**, 2464–2472.

54 I. Hod, W. Bury, D. M. Gardner, P. Deria, V. Roznyatovskiy, M. R. Wasielewski, O. K. Farha and J. T. Hupp, *J. Phys. Chem. Lett.*, 2015, **6**, 586–591.

55 C. R. Wade, M. Li and M. Dincă, *Angew. Chem.*, 2013, **125**, 13619–13623.

56 C.-W. Kung, T. C. Wang, J. E. Mondloch, D. Fairen-Jimenez, D. M. Gardner, W. Bury, J. M. Klingsporn, J. C. Barnes, R. van Duyne and J. F. Stoddart, *Chem. Mater.*, 2013, **25**, 5012–5017.

57 M. Gingras, V. Placide, J. M. Raimundo, G. Bergamini, P. Ceroni and V. Balzani, *Chem.-Eur. J.*, 2008, **14**, 10357–10363.

58 D. F. Watson and G. J. Meyer, *Coord. Chem. Rev.*, 2004, **248**, 1391–1406.

59 G. Redmond and D. Fitzmaurice, *J. Phys. Chem.*, 1993, **97**, 1426–1430.

60 B. Enright, G. Redmond and D. Fitzmaurice, *J. Phys. Chem.*, 1994, **98**, 6195–6200.

61 A. J. Morris and G. J. Meyer, *J. Phys. Chem. C*, 2008, **112**, 18224–18231.

62 C. A. Kelly, F. Farzad, D. W. Thompson, J. M. Stipkala and G. J. Meyer, *Langmuir*, 1999, **15**, 7047–7054.

63 P. Qu and G. J. Meyer, *Langmuir*, 2001, **17**, 6720–6728.

64 E. Flage-Larsen, A. Royset, J. H. Cavka and K. Thorshaug, *J. Phys. Chem. C*, 2013, **117**, 20610–20616.

65 L. M. Yang, E. Ganz, S. Svelle and M. Tilset, *J. Mater. Chem. C*, 2014, **2**, 7111–7125.

66 C. G. Silva, I. Luz, F. X. L. I. Xamena, A. Corma and H. Garcia, *Chem.-Eur. J.*, 2010, **16**, 11133–11138.

67 K. Vinodgopal, X. Hua, R. L. Dahlgren, A. G. Lappin, L. K. Patterson and P. V. Kamat, *J. Phys. Chem.*, 1995, **99**, 10883–10889.

68 K. Hashimoto, M. Hiramoto, T. Sakata, H. Muraki, H. Takemura and M. Fujihira, *J. Phys. Chem.*, 1987, **91**, 6198–6203.

69 N. Ikeda, A. Yoshimura, M. Tsushima and T. Ohno, *J. Phys. Chem. A*, 2000, **104**, 6158–6164.

70 M. J. Katz, Z. J. Brown, Y. J. Colon, P. W. Siu, K. A. Scheidt, R. Q. Snurr, J. T. Hupp and O. K. Farha, *Chem. Commun.*, 2013, **49**, 9449–9451.

71 V. Bon, I. Senkovska, M. S. Weiss and S. Kaskel, *CrystEngComm*, 2013, **15**, 9572–9577.

72 M. Inokuti and F. Hirayama, *J. Chem. Phys.*, 1965, **43**, 1978–1989.

73 G. M. Hasselman, D. F. Watson, J. R. Stromberg, D. F. Bocian, D. Holten, J. S. Lindsey and G. J. Meyer, *J. Phys. Chem. B*, 2006, **110**, 25430–25440.

74 J. N. Clifford, E. Palomares, M. K. Nazeeruddin, M. Grätzel, J. Nelson, X. Li, N. J. Long and J. R. Durrant, *J. Am. Chem. Soc.*, 2004, **126**, 5225–5233.

75 A. Schaate, P. Roy, A. Godt, J. Lippke, F. Waltz, M. Wiebcke and P. Behrens, *Chem.-Eur. J.*, 2011, **17**, 6643–6651.

